Results in Surfaces and Interfaces 13 (2023) 100147

Contents lists available at ScienceDirect

Results in Surfaces and Interfaces

journal homepage: www.elsevier.com/locate/rsurfi

Polyorganosilazane/GPTMS functionalized silica coatings as an integrated corrosion–resistance system for AA2024-T3 aluminum alloy

Udhaya Kumar Aruchamy [a,b], Emilia Merino [b], Alicia Durán [b], Maroš Eckert [d], Dušan Galusek [a,c,**], Yolanda Castro [b,*]

[a] Centre for Functional and Surface Functionalized Glass, Alexander Dubček University of Trenčín, Študentská 2, 91150 Trenčín, Slovakia
[b] Instituto de Cerámica y Vidrio (ICV), CSIC, Campus de Cantoblanco, 28049 Madrid, Spain
[c] Joint Glass Centre of the IIC SAS, TnUAD and FChPT STU, 91150 Trenčín, Slovakia
[d] Faculty of Special Technology, Alexander Dubček University of Trenčín, 91106, Trenčín, Slovakia

ARTICLE INFO

Keywords:
Corrosion
Polysilazane
GPTMS
Synthesis
Coatings
Electrochemistry

ABSTRACT

A hybrid coating based on polyorganosilazane (Durazane® 1800) combined with 3-glycidyloxypropyltrimethoxysilane (GPTMS) was successfully synthesized to improve the corrosion resistance of the AA2024-T3 aluminum alloy. The polymers were cross–linked with the addition of tetra-n-butylammonium fluoride (TBAF), and the hybrid coatings were deposited on aluminum substrates by dip coating and dried at 120 °C. Crack-free films with a thickness of 13 μm were obtained. Field emission electron microscopy (FESEM) analysis indicated that the synthesized hybrid films were smooth, homogenous, and devoid of cracks. Attenuated total reflectance Fourier transform infrared spectroscopy (ATR-FTIR) studies demonstrated that the intensity of the Si–N–Si peak was maintained, showing that the backbone of the polysilazane was preserved after the addition of GPTMS. Nuclear magnetic resonance (NMR) spectroscopy indicated that glycidoxypropyl groups were still present in the Si–O–N network of the modified polysilazane. Contact angle measurements indicated that the hybrid coatings were hydrophobic, with a measured contact angle of 93 ± 6°. The electrochemical results confirmed that the synthesized hybrid coatings improved the corrosion resistance of the aluminum substrate in 3.5 wt% NaCl solution. This suggest that the modified polyorganosilazane coating is an effective solution for developing anti-corrosive coatings on metal substrates, offering excellent adhesion strength and good scratch resistance.

1. Introduction

Aluminum and its alloys have been the primary materials of choice for the aircraft and aerospace industries for more than 80 years due to their low weight, ease of machinability, and suitable mechanical properties for supporting the design of aircraft structures and engines. The decrease in weight can reduce fuel consumption and increase payload during long flights, directly reducing operating costs (Dursun and Soutis, 2014; Zhang et al., 2018). However, its low corrosion resistance in coastal and harsh environments critically limits its use. There are different ways to enhance the corrosion resistance of aluminum alloys, but the use of surface modification techniques to avoid contact of the aluminum surface with corrosive environments is one of them. In particular, chromate conversion coatings (CCC and CCA) represent the most efficient and low-cost strategies. However, the restrictions relating to the use of hexavalent chromium Cr (VI) as a surface treatment are extremely strict due to its health and environmental risks. Although aircraft or aerospace companies continue to use hexavalent chromium in specific applications, efforts are underway to identify alternative and effective environmental surface treatments. For example, some companies have started with the development and marketing of trivalent chromium coatings that are less toxic (<0.1 wt% set by REACH regulations (Ely et al., 2017)). Other research groups have been working on developing conversion coatings based on heteropolymetalates or polymetalates such as heteropolymolybdates, where Mo (III) and Mo (IV) are transformed to Mo (V) and M (VI) species that are more stable (Minevski et al., 2002). Despite these efforts, a complete replacement of Cr^{+6}-based coatings have not yet been achieved, and it remains uncertain whether such a replacement is feasible. However, various alternatives can be considered and used for many applications, depending on each specific

* Corresponding author. Instituto de Cerámica y Vidrio (ICV), CSIC, Campus de Cantoblanco, 28049 Madrid, Spain.
** Corresponding author. Centre for Functional and Surface Functionalized Glass, Alexander Dubček University of Trenčín, Študentská 2, 91150 Trenčín, Slovakia.
E-mail addresses: dusan.galusek@tnuni.sk (D. Galusek), castro@icv.csic.es (Y. Castro).

https://doi.org/10.1016/j.rsurfi.2023.100147
Received 13 July 2023; Received in revised form 1 September 2023; Accepted 11 September 2023
Available online 21 September 2023

coating, and here the sol–gel process emerged as a facile and versatile technology. The sol–gel process is considered a very efficient and economical solution for developing anti-corrosive coatings on metal substrates. According to Segal (1984), "the term sol-gel processing usually refers to the fabrication of inorganic oxides using either metal alkoxide precursors or colloidal dispersions (sols) of hydrous oxides". Polysiloxanes (Si–O–Si) sol–gel coatings have been proposed as a suitable alternative for chromate conversion coatings (Castro et al., 2020; Arunoday et al., 2022; Mussa et al., 2021; Subasri et al., 2019). Thus, numerous papers (Salstela et al., 2016; Feng et al., 2010; Ochi et al., 2001) have reported promising anti-corrosive properties and adequate adherence to aluminum substrates of hybrid silica coatings obtained using different organic silane monomers, particularly glycidoxypropyltrimethoxysilane (GPTMS) (Salstela et al., 2016; Feng et al., 2010; Ochi et al., 2001). The organic component of these hybrid materials can improve the adhesion, density, and flexibility of the coating, while the inorganic component can enhance scratch resistance, thermal stability, hardness, optical characteristics, and corrosion resistance (Arunoday et al., 2022; Xiong et al., 2019; Zhang et al., 2023).

Despite their remarkable barrier properties, inorganic-organic hybrid coatings can suffer from mechanical damage and defects when exposed to harsh environments or during transportation and service life (Segal, 1984). The presence of defects in the coatings results in a quick diffusion of electrolyte through micropores or scratches, accelerating the degradation of the aluminum substrate. The economic cost associated with corrosion failure is costly and cumbersome. Currently, different approaches have emerged to improve the corrosion protection associated with the enhanced mechanical and thermal properties of hybrid sol-gel coatings (Askarnia et al., 2021; Askarnia et al., 2023; Sobhani et al., 2023; D'Orazio et al., 2023).

Among them, the use of polysilazanes as silicon-based polymers could be a good alternative to improve the barrier properties of sol-gel coatings. The polymer can be heat treated at temperatures $\geq$400 °C in air, N_2, and Ar atmospheres to convert it into Si_3N_4, SiCNO, SiON, or SiCN (Barroso et al., 2020), producing polymer-derived ceramics (PDC). A strong adhesion to most substrates (Picard et al., 2015; Amouzou et al., 2014) and a high chemical (Coan et al., 2015), thermal (Gardelle et al., 2011), and UV resistance (Hu et al., 2009) are some of the special properties of PDC coatings. It is crucial to control the crosslinking of polysilazane molecules without breaking them, which can be achieved using various methods including chemical reactions with the atmosphere, UV irradiation, and high-temperature treatment (600–1000 °C). In all cases, the principal objective is to obtain crack-free coatings with good chemical and mechanical properties (Flores et al., 2013; Chavez et al., 2011; Bahloul et al., 1993; Gü et al., 2012). However, large shrinkage associated with the transformation of a polymer to ceramic takes place at elevated temperatures, and during this process, cracks or pores can be formed. Therefore, achieving defect-free coatings with excellent chemical and mechanical properties at low sintering temperatures is crucial (Zhang et al., 2023; Askarnia et al., 2021, 2023; Sobhani et al., 2023) to protecting light alloys such as aluminum or magnesium alloys. For instance, Bauer et al. (2005) reported a novel method for preparing silazane-based coatings employing moisture and low heat-treatment (50–100 °C). According to their results, the curing mechanism is based on the condensation of silanols produced by the hydrolysis reactions of Si–H and Si–N with the OH groups in moisture. They also claimed that the inclusion of polyorganosilazane moieties provides an opportunity to improve the hardness and flexibility of the polysilazane films (Bauer et al., 2005). Similarly, Nicolas et al. (Dargè et al., 2012) investigated the hydrolysis and condensation reactions of an organosilazane molecule (1,1,3,3-tetramethyldisilazane) with water at room temperature and suggested that Si–N groups hydrolyze faster than the Si–H groups, resulting in the formation of Si–N–Si and Si–O–Si polymer networks.

Dense coatings at low temperatures ($\leq$100 °C) have been reported with the addition of catalysts such as 1,2,4-triazole compounds (Hafidh et al., 2020), chloroplatinic acid (H_2PtCl_6) (Yuan et al., 2019), dicumyl peroxide (DCP) (D'Elia et al., 2018), and tetra-n-butylammonium fluoride (Furtat et al., 2017; Zhan et al., 2021). Another strategy involves modifying the polysilazane backbone by introducing organic functional groups to achieve dense polysilazane-derived coatings. Trifluoroethoxy, vinyl, hydroxyl, monomethoxy, and methyl methacrylate have been considered Si–O–N network modifiers (Coan et al., 2015; Lo et al., 2020; Perrin et al., 2015; Nguyen et al., 2013; Kong et al., 2013). In all cases, the modified polysilazane solutions can be deposited and cured on metal substrates at low temperatures. For example, Corriu et al. (1983) developed a novel method that utilizes nucleophilic catalysts to synthesize polysilazane coatings on metallic substrates. This approach has demonstrated potential for achieving excellent corrosion–resistant properties without decomposing the silazane backbone. However, the synthesis process can be complex, which can limit control over the resulting coating's structure. Furtat et al. (2017) prepared coatings on AISI 304LN and aluminum substrates using Durazane 1800 modified with trifluoroethoxy functional groups with remarkable oxidation resistance and a high contact angle. However, despite the numerous papers related to the use of hybrid silica sol-gel coatings to control the corrosion of aluminum alloys, there are very few references to polyorganosilazanes–based coatings. The inclusion of organic substituents in the polysilazane polymer allows adjustment of its properties.

Thus, the aim of the present study was to examine the incorporation of GPTMS precursor into polyorganosilazane networks to improve the corrosion resistance of aluminum alloys. To the best of our knowledge, this is the first time a modified polyorganosilazane has been used to coat the AA2024-T3 alloy. The modified polyorganosilazane solution was prepared in the presence of TBAF as a nucleophilic catalyst to obtain a pre-crosslinked polyorganosilazane backbone and to avoid decomposition of the polymer. Attenuated total reflectance Fourier transform infrared spectroscopy (ATR-FTIR) and nuclear magnetic resonance (NMR) were used to study the effects of synthesis steps on chemically modified structures. The resulting anti–corrosive properties of modified polyorganosilazane coatings were assessed using electrochemical impedance spectroscopy (EIS) and potentiodynamic polarization (PDP) tests in a 3.5 wt% NaCl solution, showing an improvement in corrosion resistance. The modified polyorganosilazane coatings exhibited favorable hydrophobic and mechanical properties, including excellent adhesion strength to AA2024 and good scratch resistance.

2. Materials and methods

2.1. Materials

Durazane® 1800 designated as polyorganosilazane (OPSZ), and n-butyl acetate (NBTA, 99%) were supplied by Merck, Germany. 3-(glycidyloxypropyl) trimethoxysilane (GPTMS, 98%) was provided by ABCR, Germany. Tetra-n-butylammonium fluoride (TBAF), 1M in tetrahydrofuran (THF), was received from Alfa Aesar, USA. All reactants were used without further purification.

2.2. Pre–treatments

Prior to the coating, a commercially available aluminum alloy (AA2024-T3) with a composition (wt%) of 4.67% Cu, 0.05% Si, 0.21% Fe, 1.5% Mg, 0.64% Mn, 0.029% Ti, 0.07% Zn, (Al was the rest) was cut to the dimensions of 2 × 4 × 0.2 cm^3, and pre–cleaned using the procedure reported in (Castro et al., 2020). Then, the samples were rinsed with acetone, deionized water, and dried in ambient air.

2.3. Synthesis of modified polysilazanes solution

8 g of Durazane® 1800 was dissolved in 6.4 g of n-butyl acetate (NBTA). After stirring for 20 min at 25 °C, 0.5 wt% TBAF was added dropwise to prevent OPSZ fragmentation and evaporation. Then, 15 wt

% of GPTMS (relative to OPSZ) was added to the reaction mixture and refluxed at 55 °C for 60 min under continuous magnetic stirring. Finally, a transparent and yellow solution was obtained and maintained at RT. Fig. 1 illustrates the synthesis of polyorganosilazane/GPTMS sol.

A similar procedure was used to prepare a polyorganosilazane solution without the addition of GPTMS.

2.4. Characterization of the modified polysilazane solution

The presence of reactive groups and their crosslinking during the synthesis of modified polysilazane solutions were monitored by a Fourier transform infrared spectrophotometer (a PerkinElmer Spectrum 100 spectrometer with a diamond ATR sampling unit). The spectrum was recorded between 4000 and 400 cm^{-1} using 16 scans at a resolution of 0.5 cm^{-1}. A Bruker Avance-400 pulse spectrometer (Karlsruhe, Germany) was employed to obtain solid-NMR spectra. ^{13}C CP-MAS spectra were measured to provide structural characterization of the polyorganosilazane/GPTMS sol cured at 120 °C. The spectra were recorded after irradiation of samples with a π/2 (5 μs) pulse in a single pulse sequence. In order to avoid saturation effects, the recycle delay times used were 10 s. The spinning rate used in MAS-NMR experiments was 10 kHz. The number of scans was varied between 400 and 800. All measurements were carried out at room temperature with TMS (tetramethylsilane) as an external standard. The error in chemical shift values was estimated to be lower than 0.5 ppm.

2.5. Coating deposition

The synthesized polyorganosilazane/GPTMS and polyorganosilazane sols were deposited onto the pre–cleaned AA2024-T3 alloy by dip–coating using a withdrawal rate of 30 cm/min. Then, the coated Al substrates were heat treated at 120 °C for 2 h. The resulting coatings were labeled as OPSZ/GPTMS coating and OPSZ coating, respectively.

2.6. Coating characterization

The surface topography and elemental composition of the OPSZ/GPTMS coatings were examined using field emission scanning electron microscopy (FESEM) equipped with an energy-dispersive X-ray spectroscopy (EDS) detector (model: Hitachi S4700). The FESEM was operated at an acceleration voltage of 20 kV, while the EDS detector was operated at 5 kV.

The surface roughness (Ra-parameter) was measured using a profilometer (Model: Zeta 20, KLA Corporation) at a magnification of 20× and a resolution of 0.1 nm. Contact angle measurements of both bare and coated aluminum substrates were carried out using the dynamic sessile drop method (model: Kruss DSA 100) in an ambient atmosphere, depositing around 4 μL of water on the surface. To minimize errors and increase the reliability of the results, repeated measurements were performed on each sample.

The corrosion protection properties of the OPSZ/GPTMS and OPSZ films were evaluated using potentiodynamic polarization and electrochemical impedance spectroscopy (EIS) techniques. A saturated calomel electrode (SCE) was used as the reference electrode, a platinum wire electrode as the counter electrode, and coated and uncoated AA2024-T3 samples as the work electrode. To reach a steady state condition, the open circuit potential (E_{oc}) was recorded for 3600 s before polarization curves and EIS spectra measurements. Potentiodynamic polarization curves (PDPs) were recorded by varying the potential from −500 mV up to +500 mV related to the saturated calomel electrode (SCE) and applying the sweep rate of 1 mV/s in 3.5 wt% NaCl, using a Gamry Instruments (PA, USA) electrochemical cell. The exposed area was fixed to 0.78 cm^2. The corrosion potentials (E_{corr}) and corrosion current densities (i_{corr}) were determined from potentiodynamic polarization curves using Tafel extrapolation.

The EIS measurements were performed in the frequency range of 1×10^5 Hz–0.1 Hz at OCP by applying an AC voltage amplitude of 10 mV. Gamry Echem Analyst software (Gamry Instrument, Inc.) was used to analyze and fit the PDP and EIS data. The experiments were repeated at least three times to verify their reproducibility. Before and after the EIS measurements, the samples were analysed by visual observation using a digital camera.

Dry sliding wear tests were performed using a pin-on-disc tribometer (MT/10/SCM from Microtest). The slider disc was a 100 Cr steel ball with a 6 mm diameter. The test parameters were a normal load of 1 N and a total sliding distance of 40 m with a rotating speed of 0.01ms^{-1}. Finally, the scratch resistance (CETR/MOD: MM-1) of the coated substrates was determined by generating a controlled scratch with a diamond tip over the specimen surface. The tip was drawn across the coated surface under constantly increasing loads. The normal applied load ranged from 0 to 10 N and the scratch speed was 0.025 mm/s. At the

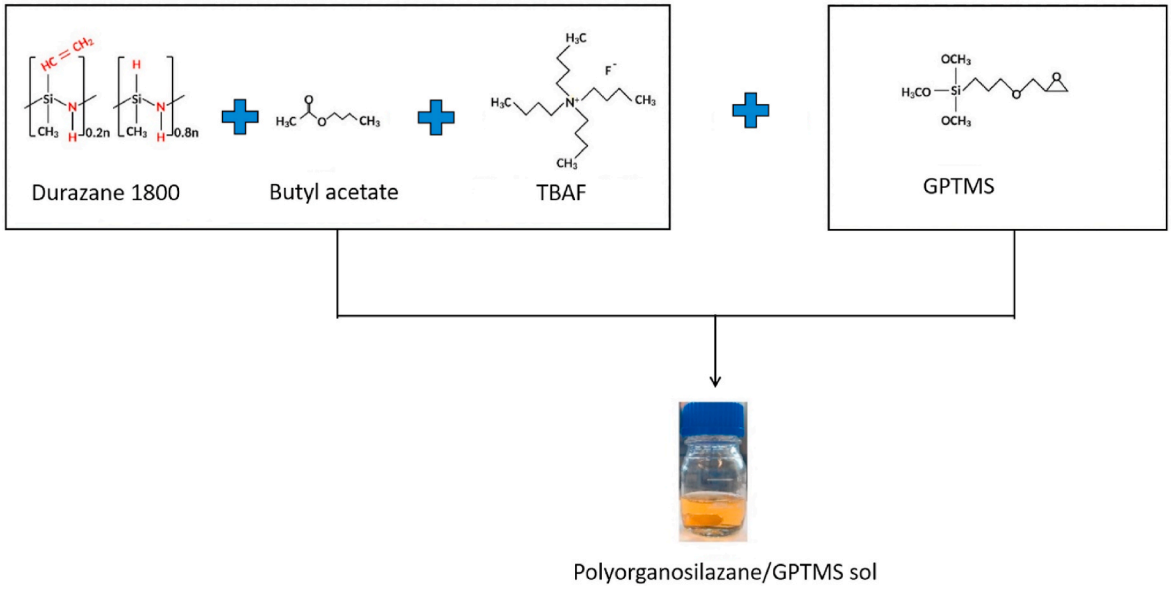

Fig. 1. Flow chart of the synthesis of polyorganosilazane/GPTMS sol.

critical load, coating failure was discerned by optical microscopy of the surface during testing. 2–3 different tests were performed to determine the reproducibility.

3. Results and discussion

We initially diluted OPSZ in NBTA (**OPSZ + NBTA**), and then, TBAF **(OPSZ + NBTA + TBAF)** was added to the mixture. Finally, GPTMS was added and heated for 1 h at 55 °C (**OPSZ + NBTA + TBAF + GPTMS**). During the synthesis, liquid samples were collected and analysed using FTIR to investigate the reaction mechanism of the modified polyorganosilazane solutions in detail. The principal bands at ~3380 cm^{-1} (N–H stretching mode), ~1165 cm^{-1} (N–H bending mode), ~2119 cm^{-1} (Si–H symmetric deformation), ~880 cm^{-1} (Si–N–Si symmetric stretching mode), ~1260 cm^{-1} (CH_3 of the non–hydrolysable Si–CH_3 group), and ~1403 cm^{-1} (C═C vibrations), associated with the OPSZ precursor, were identified in the spectra (Dursun and Soutis, 2014; Zhang et al., 2018) (Fig. 2a). The –CH_2 band (~1403 cm^{-1}) was used as an internal standard to compare the spectra because this band does not undergo modifications during the synthesis.

Fig. 2 (b–d) shows the area magnification of the most important peaks. The spectrum of OPSZ + NBTA + TBAF exhibits three significant changes in comparison with the OPSZ + NBTA spectrum. The intensities of N–H (~1165 cm^{-1}) and Si–H (~2119 cm^{-1}) bands decreased, and the intensity of the Si–N band (880 cm^{-1}) increased, indicating that the TBAF catalyzed the dehydro–coupling reaction between Si–H and N–H to yield new Si–N–Si bonds (Flores et al., 2013; Furtat et al., 2017). The inclusion of TBAF is also essential for enhancing the Si–H bond reactivity and preventing the decomposition of the silazane backbone induced by water impurities during synthesis (Segal, 1984).

With the addition of GPTMS, a new small band at 1089 cm^{-1} (Fig. 2d), assigned to its corresponding Si–O–CH_3 stretching vibration mode, was identified (Segal, 1984). However, the intensity of the Si–H, N–H, and Si–N–Si bands did not change, indicating that GPTMS did not react with the silazane molecule in the liquid state. However, after curing the sol at 80 °C, significant changes were observed in the FTIR spectra. Fig. 3 shows the spectra of the cured OPSZ + NBTA + TBAF and OPSZ + NBTA + TBAF + GPTMS samples.

The reduction of the intensity of the Si–H peak and the appearance of a broad band around 1020 cm^{-1} corresponding to Si–O–Si bonds indicate that the GPTMS molecule was bound to the silazane backbone by hydrolysis and condensation between the Si–OEt and Si–H groups. Lo et al. (2022), reported the formation of silanol groups (CH_3–Si–OH) due to a rapid reaction of CH_3–Si–H groups with a small amount of water. Then, the Si–OEt group can condense, forming Si–O–Si bonds associated with the humidity presence in the environment during the curing

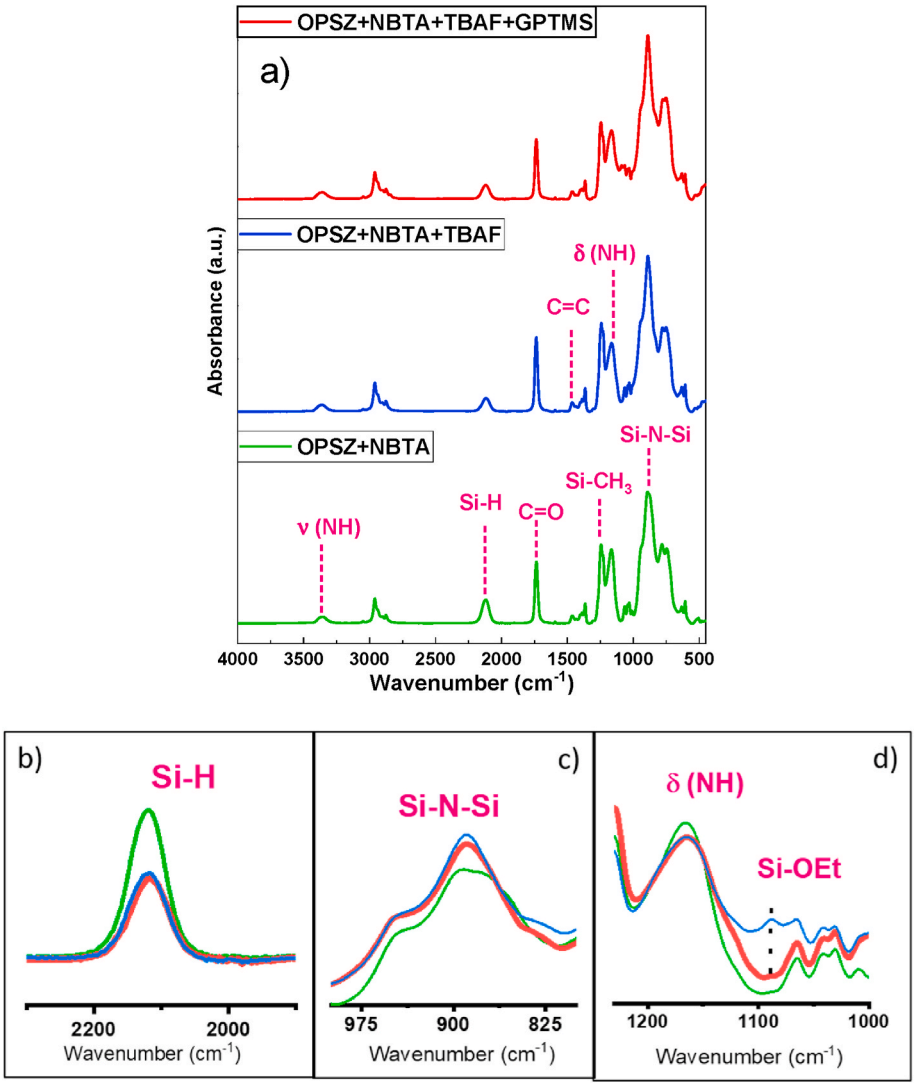

Fig. 2. FTIR spectra of OPSZ + NBTA, OPSZ + NBTA + TBAF and the modified polyorganosilazane (a). Si–H (b), N–H bending mode, Si–OEt (c) and Si–N–Si (d) bands in detail.

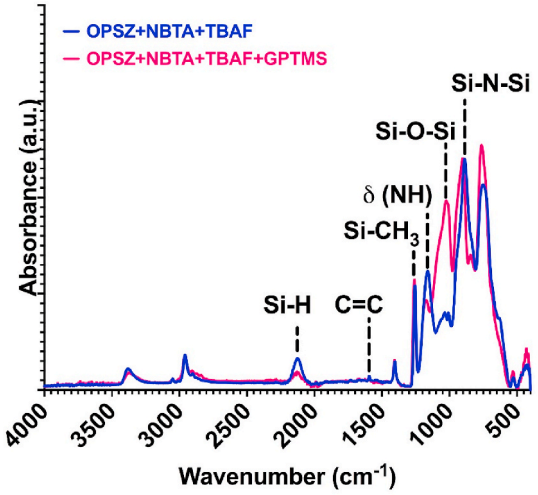

Fig. 3. FTIR spectra of OPSZ + NBTA + TBAF and OPSZ + NBTA + TBAF + GPTMS after curing at 80 °C.

process, releasing hydrogen and ethanol. As Si–H and Si–NH are two types of bonds with similar bond energies of 378 and 437 kJ mol^{-1} (Sønderbæk-Jø et al., 2022), the moisture in the environment can also react with the Si–NH–Si bonds to produce Si–NH_2, OH–Si, and NH_3 as by products. The release of ammonia leads to an alkaline environment that can catalyze the hydrolysis and self-condensation of Si–OH and Si–OEt groups (Dargè et al., 2012; Marceaux et al., 2014) to form more Si–O–Si bonds. The reduction of the intensity of the Si–NH peak suggests that GPTMS aids in the hydrolysis and condensation of the Si–NH–Si bonds, leading to the formation of additional Si–O–Si bonds (Fig. 3), as mentioned by Müller et al. (Mü et al., 2016). The intensity of Si–N–Si peak is maintained, indicating that the backbone of the polysilazane is preserved after GPTMS addition (Fig. 3). These findings demonstrate that at low temperatures (80 °C) the curing mechanism promotes the hydrolysis and condensation reactions between Si–H, Si–NH, and Si–OEt bonds, resulting in the development of a cross–linked Si–O–N network composed of Si–N–Si and Si–O–Si bonds.

Further information about the Si–O–N network structure was obtained using ^{13}C MAS NMR spectroscopy. Fig. 4 shows the NMR spectra of ^{13}C of the OPSZ + NBTA + TBAF + GPTMS sample after curing at 120 °C. Different ^{13}C NMR signals (Fig. 4) were assigned based on the data from the literature (Gardelle et al., 2011; Dargè et al., 2012; Yokota et al., 2010; Wang et al., 2022; Templin et al., 1997). The signals

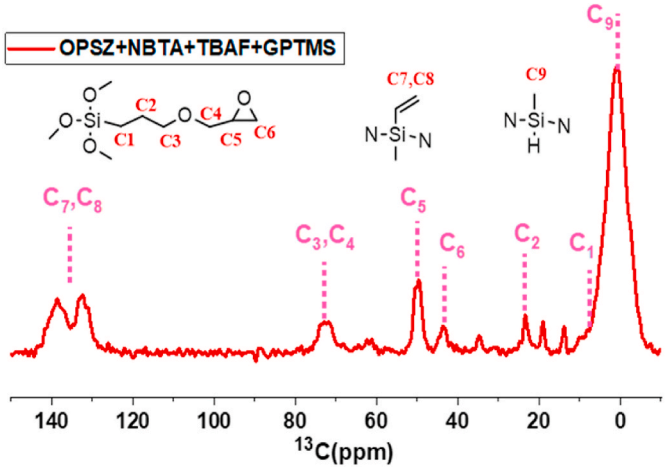

Fig. 4. ^{13}C MAS NMR spectra of a PSZ + NBTA + TBAF + GPTMS sample after curing at 120 °C.

associated with the carbon atoms of the GPTMS and OPSZ molecules (designated from C_1 to C_9) were identified.

The signals corresponding to C═C (C_7, C_8) and Si–CH_3 (C_9) of the OPSZ molecule were detected in the range of 140–120 ppm and 7–5 ppm, respectively. Two other peaks at 51.2 ppm and 44.3 ppm, corresponding to –CHO– (C5) and –OCH_2– (C6), associated with the epoxy ring of GPTMS, were also identified. This demonstrates that epoxy groups remain in the Si–O–N network of the modified polyorganosilazane polymer after the curing procedure. The peak associated with the C═O group of the NBTA is not detected due to the drying process at 120 °C for 2 h that results in the removal of the solvent.

FESEM images were taken to examine the morphology and cross–section of the polyorganosilazane/GPTMS coating on the AA2024–T3 substrate (labeled as OPSZ/GPTMS coating) after heat treatment at 120 °C for 2 h in air. Fig. 5a shows a smooth, homogeneous, and crack-free surface coating. Moreover, the cross-section image (Fig. 5b) shows that the OPSZ/GPTMS coating adheres well to the substrate, with a coating thickness of approximately 13 μm. The elemental composition of the coating and substrate was analysed using EDS mapping of the same zone as in the cross-section image (Fig. 5c). The elemental mapping corroborated the presence of aluminium in the substrate (yellow) and Si in the coating (purple).

Average surface roughness (R_a) and contact angle measurements were carried out on bare and OPSZ/GPTMS coated Al substrates. The deposition of the coating significantly decreases the surface roughness, Ra (arithmetical mean deviation), from 4.0 ± 0.4 to 0.2 ± 0.6 μm, for bare and coated Al substrates, respectively. The contact angle value was also measured with water, and values of 93 ± 6° for the coated sample and 46° ± 8 for the bare AA2024-T3 substrate were obtained. The deposition of a OPSZ/GPTMS coating results in an increased contact angle compared to the bare AA2024-T3 substrate, probably due to the presence of Si–CH_3 and Si–CH═CH_2 groups that do not participate in the crosslinking reactions at room temperature (RT) and their low surface energy. This is expected to result in higher corrosion resistance.

Electrochemical studies were performed to analyze the corrosion behaviour of the blank and OPSZ/GPTMS coating and to compare it with an OPSZ coating obtained without the incorporation of GPTMS. The results of potentiodynamic tests are shown in Fig. 6. The anodic and cathodic branches shift to lower current densities for both coated substrates, indicating that the corrosion rate is lower than that of the bare AA2024-T3 substrate.Furthermore, a broad passive range (ΔE) was observed, indicating that the coatings are stable against pitting corrosion and spontaneous degradation (Zhang et al., 2005). However, the i_{corr} for the OPSZ/GTPMS coated substrate is three order of magnitude lower than that of the OPSZ coating. Specifically, the OPSZ/GTPMS coating shows an i_{corr} value of $\sim 10^{-10}$ A/cm^2 compared to $\sim 10^{-7}$ A/cm^2 for the OPSZ/GPTMS coating, suggesting better corrosion resistance for the OPSZ/GPTMS coating. Overall, these results strongly indicate the enhanced corrosion resistance of OPSZ/GPTMS coating.

The electrochemical impedance spectroscopy technique was used to assess the corrosion resistance properties of the OPSZ/GPTMS coating during immersion in a 3.5 wt% NaCl solution. Fig. 7a shows the impedance spectra of coated and uncoated samples, with impedance magnitude (Ohm) plotted against frequency (Hz).

The impedance modulus |Z| in a low frequency domain (f < 1 Hz) and the phase angle graph can be used to estimate the difference in anti-corrosive performance between the hybrid coating and the bare Al alloy. The impedance modulus value of the coated sample was $\sim 10^9$ Ω cm^2 in the frequency range <1 Hz, which is about five orders of magnitude higher than that of the bare aluminium alloy, $\sim 10^4$ Ω cm^2 (Fig. 7a). The capacitive phase angle value of the coating is close to −90° indicating a highly capacitive behaviour during the initial immersion period (1 h) and confirming its high–performance in protecting the substrate against corrosion (Hintze and Calle, 2006; Nguyen et al., 2017). To obtain quantitative information on the electrochemical processes taking place on the coated metal surface over a longer immersion

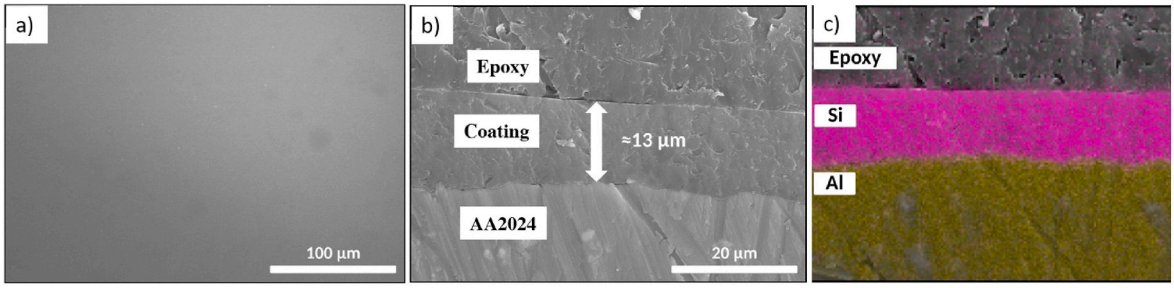

Fig. 5. FESEM images of the surface (a), cross-sectional image (b), and an EDS analysis (c) of AA2024 alloy coated with a polyorgansilazane/GPTMS coating.

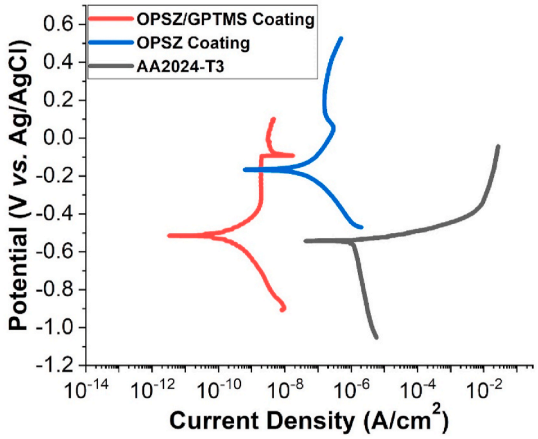

Fig. 6. Potentiodynamic polarization curves of OPSZ and OPSZ/GPTMS coated Al substrates compared to AA2024–T3 in 3.5 wt% NaCl.

time, the EIS data were fitted using electrical equivalent circuits (EC), as presented in Fig. 7b. In general, these equivalent circuits are based on the combination of resistance and capacitance elements that describe electrochemical phenomena occurring at the electrolyte/(OPSZ/GPTMS) film/metal interface after 1 h, 48 h, and 168 h of immersion. Table 1 presents the numerical fitting values obtained for the different spectra at different immersion times. The total corrosion resistance values (R_p) were calculated as the sum of all the faradaic resistances according to the fitted values given in Table 1.

During the first hour of immersion, the coating appears to act as a physical barrier since the Rp value is high ($\sim 10^9\ \Omega\ cm^2$) and a one–time constant EC model, corresponding to the resistance and capacitance of the OPSZ/GPTMS coating (R_{SG}, CPE_{SG}), is sufficient to describe the material behaviour. At this point, the low CPE value of about $10^{-10}\ \Omega^{-1}\ cm^{-2}\ s^{\alpha coat}$ indicates low water transportation through the film, likely due to the hydrophobicity of the coating (contact angle >90°) which restricts the corrosive attack on the substrate. As the immersion time is extended to 48 h, the electrolyte penetrates towards the interlinked hybrid network, and the Rp value decreases to $\sim 10^8\ \Omega\ cm^2$ due to the formation of pores or channels in the sol-gel derived coating. It is then necessary to use a two-time-constant EC model where the first time constant represents an outer layer with the presence of pores (R_{out} and CPE_{out}), while the second time constant corresponds to the preserved inner layer with high impedance (R_{in} and CPE_{in}). After a longer period of time, 168 h, the percolation of the corrosive electrolyte into the coating creates more channels, and the capacitance of the inner layer increases from $\sim 10^{-9}\ \Omega^{-1}\ cm^{-2}\ s^{\alpha coat}$ to $\sim 10^{-8}\ \Omega^{-1}\ cm^{-2}\ s^{\alpha coat}$ and the R_P value drops to $\sim 10^{-9}\ \Omega\ cm^2$. Additionally, a third time–constant (R_{dl} and CPE_{dl}) appears to represent the charge transfer resistance and the double layer capacitance between the electrolyte and the substrate, indicating a failure of the coating.

Although, the overall protection ability of the coating gradually decreases with time due to water and ion permeation, the presence of the epoxy group in the film documented by the ^{13}C NMR spectra opens a promising new work line in the surface–coating field to obtain a more highly cross-linked network through organic polymerization and, thus, more efficient corrosion protection for prolonged immersion.

Fig. 7c and d shows the visual images obtained by a digital camera for the OPSZ/GPTMS coated substrate before and after the EIS test in a 3.5 wt% NaCl solution, respectively. Before the inmersion, a transparent and defect-free coating is observed on the AA2024-T3 substrate. However, after 168 h of immersion in NaCl, a small pitting corrosion is detected (Fig. 7d, marked with a dotted circle), corroborating the slight decrease of the impedance module at low frequency. Although the extent of the corrosion damage is remarkably small.

The mechanical properties of the film are significantly influenced by the cross-linking of the network and by the sintering condition of the coating. Fig. 8 shows the change in the friction coefficient (CoF) with the sliding distance for the uncoated and coated substrates. The coated sample shows a different tendency than the uncoated sample. The initial CoF of the coated AA2024 (0.036) is one order of magnitude lower than that presented for the uncoated alloy (0.147). This low CoF is attributed to the excellent abrasive resistance of the coated sample, which is likely due to the presence of Si–N–Si and Si–O–Si backbone of the inorganic network. Then, the friction coefficient of the uncoated sample increases with distance up to a maximum of 0.5, while in the case of the coated sample, it is maintained constant up to a distance of 20 m, indicating that the deposition of a coating can prevent the scratching and cutting of the surface. In the case of the coated sample, the contact with the grinding ball becomes larger, leading to a reduction in the wear resistance properties, which in turn causes an increase in the friction coefficient. However, the coating significantly enhances the wear resistance of the uncoated sample, at least up to a sliding distance of 20 m.

Fig. 9 shows the optical image of the wear track after the scratch test, along with the variation of the load and friction coefficient (CoF) as a function of sliding distance for the OPSZ/GPTMS coated sample. Two critical loads are observed in Fig. 9: the cohesive failure (L_{c1}), associated with the appearance of the first cracks or failures in the coating, and the supercritical load (L_{c2}), associated with the delamination and detachment of the coating from the substrate (Egorkin et al., 2016; Macá et al., 2019). The film-based bonding force exhibits a gradually increasing trend until it reaches L_{c1} of 6.3 N and L_{c2} of 7.8 N, respectively. This indicates that the coating system demonstrates greater coating adhesion compared to previous reports (Ló et al., 2015; Sowntharya et al., 2013).

4. Conclusions

This study has successfully demonstrated the synthesis of a novel formulation of polyorganosilazane/GPTMS sol using tetrabutylammonium fluoride (TBAF) as a catalyst, resulting in a homogeneous and crack–free coating on an AA2024 aluminum alloy substrate with a thickness of 13 µm. As documented by the ATR-FTIR, the addition of TBAF decreases the content of Si–H and Si–NH bonds, favoring the formation of new Si–N groups. Further addition of GPTMS to OPSZ +

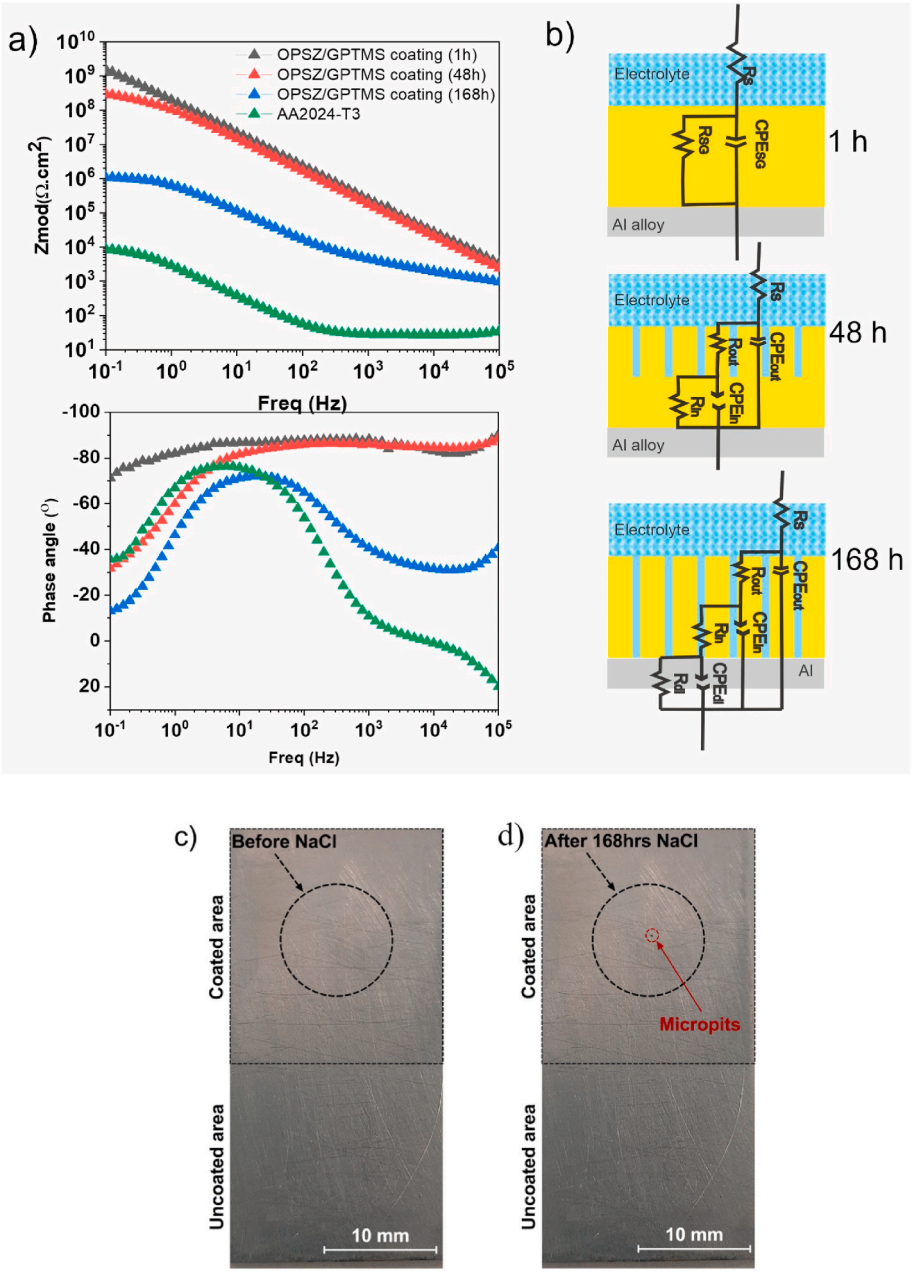

Fig. 7. Bode and phase angle plots of coated and uncoated samples (a). Equivalent circuit model (b) for the coated samples following immersion times of 1h, 48h and 168h and visual images of coated sample c) before and d) after 168 h of immersion in 3.5 wt% NaCl (c).

NBTA + TBAF solution did not change the intensity of the Si–H, N–H, and Si–N–Si bands, indicating that GPTMS did not react with the silazane molecule in the liquid state. After curing at 80 °C, hydrolysis and condensation reactions between Si–H, Si–NH, and Si–OEt bonds are promoted, culminating in the development of a cross–linked Si–O–N network composed of Si–N–Si and Si–O–Si links. The resulting polyorganosilazane/GPTMS coatings exhibit favorable mechanical properties, including excellent adhesion strength to AA2024 and good scratch resistance, while also reducing and controlling the corrosion of Al alloys. These findings support the potential of polyorganosilazane/GPTMS coatings as environmentally friendly barrier coatings for a variety of applications.

This study has provided a foundation for further research to optimize the coating process and enhance the performance of these coatings, ultimately leading to more sustainable and efficient solutions for protecting metallic substrates in harsh environments. The potential of OPSZ/GPTMS coatings to provide corrosion protection and mechanical durability makes them an attractive option for a variety of industrial applications.

CRediT authorship contribution statement

Udhaya Kumar Aruchamy: Investigation, Data curation, Writing – original draft, Writing – review & editing. **Emilia Merino:** Investigation, Data curation, Writing – original draft, Writing – review & editing. **Alicia Durán:** Conceptualization, Data curation, Visualization, Writing – review & editing. **Maroš Eckert:** Visualization, Investigation. **Dusan Galusek:** Conceptualization, Methodology, Data curation, Supervision, Funding acquisition, Writing – review & editing. **Yolanda Castro:** Conceptualization, Methodology, Data curation, Supervision, Writing – original draft, Writing – review & editing.

Table 1
Fitted parameter values using the EC model presented in Fig. 7(b).

		OPSZ/GPTMS_1h	OPSZ/GPTMS _48h	OPSZ/GPTMS _168h
R_{SG}	Ω cm^2	$5.4 \times 10^9 \pm 5.5 \times 10^9$	–	–
CPE_{SG}	Ω^{-1} cm^{-2} $s^{\alpha SG}$	$8.9 \times 10^{-10} \pm 1.2 \times 10^{-11}$	–	–
	αSG	$0.9 \pm 1.7 \times 10^{-3}$	–	–
R_{in}	Ω cm^2	–	$2.0 \times 10^8 \pm 7.7 \times 10^6$	$1.7 \times 10^4 \pm 1.2 \times 10^3$
CPE_{in}	Ω^{-1} cm^{-2} $s^{\alpha in}$	–	$1.3 \times 10^{-9} \pm 8.2 \times 10^{-12}$	$7.8 \times 10^{-8} \pm 6.9 \times 10^{-9}$
	αin	–	$0.9 \pm 6.9 \times 10^{-3}$	$0.8 \pm 7.2 \times 10^{-3}$
R_{out}	Ω cm^2	–	$3.7 \times 10^8 \pm 3.8 \times 10^8$	$1.8 \times 10^4 \pm 1.2 \times 10^3$
CPE_{out}	Ω^{-1} cm^{-2} $s^{\alpha out}$	–	$5.9 \times 10^{-9} \pm 3.0 \times 10^{-10}$	$3.78 \times 10^{-9} \pm 1.0 \times 10^{-9}$
	αout	–	$0.7 \pm 6.6 \times 10^{-2}$	$0.8 \pm 2.7 \times 10^{-2}$
R_{dl}	Ω cm^2	–	–	$1.9 \times 10^6 \pm 1.0 \times 10^4$
CPE_{dl}	Ω^{-1} cm^{-2} $s^{\alpha dl}$	–	–	$5.5 \times 10^{-8} \pm 5.3 \times 10^{-9}$
	αdl	–	–	$0.9 \pm 1.3 \times 10^{-2}$
Rp	Ω cm^2	5.4×10^9	5.4×10^8	1.9×10^6

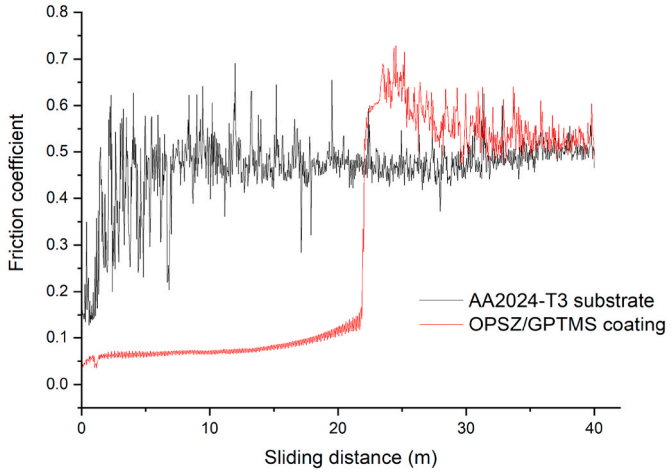

Fig. 8. Friction coefficient variation for bare and OPSZ/GPTMS coated AA2024 alloys under specific test conditions: sliding distance of 40 m. Fn: 1N, circumference velocity: 0.01 ms^{-1}.

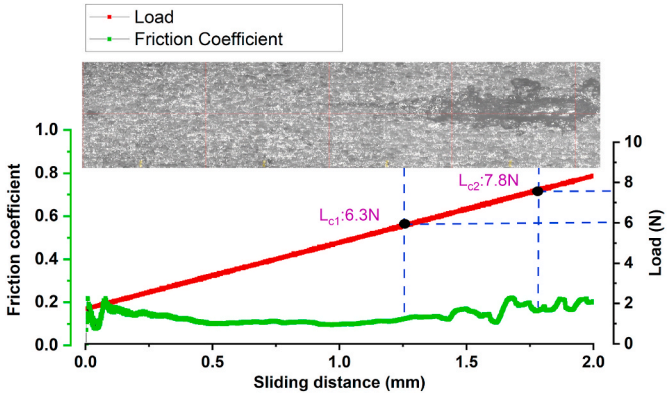

Fig. 9. Friction coefficient (CoF) variation and critical load *vs.* sliding distance, and the optical micrograph of the wear track of the scratch test for the coated sample.

Declaration of competing interest

The authors declare that they have no known competing financial interests or personal relationships that have appeared to influence the work reported in this paper.

Data availability

Data will be made available on request.

Acknowledgments

The research was funded by the European Union's Horizon 2020 research and innovation programme under the H2020 project FunGlass (Centre for Functional and Surface Functionalized Glass) [grant agreement No. 739566] and the TED2021-131258B-I00, funded by MCIN/AEI/10.13039/501100011033 and by the European Union "NextGenerationEU"/PRTR».

References

Amouzou, D., Fourdrinier, L., Maseri, F., Sporken, R., 2014. Formation of Me–O–Si covalent bonds at the interface between polysilazane and stainless steel. Appl. Surf. Sci. 320, 519–523. https://doi.org/10.1016/j.apsusc.2014.09.109.

Arunoday, M., Premkumar, K.P., Kumar, R., Subasri, R., 2022. Multifunctional, environmental coatings on AA2024 by combining anodization with sol-gel process. Ceram. Int. 48, 10969–10978. https://doi.org/10.1016/j.ceramint.2021.12.316.

Askarnia, R., Fardi, S.R., Sobhani, M., Staji, H., 2021. Ternary hydroxyapatite/chitosan/graphene oxide composite coating on AZ91D magnesium alloy by electrophoretic deposition. Ceram. Int. 47, 27071–27081. https://doi.org/10.1016/j.ceramint.2021.06.120.

Askarnia, R., Sobhani, M., Zare, M., Aghamohammadi, H., Staji, H., 2023. Incorporation of Al2O3 and ZrO2 ceramics to AZ31 magnesium alloys composite coating using micro-arc oxidation method. J. Mech. Behav. Biomed. Mater., 105784 https://doi.org/10.1016/j.jmbbm.2023.105784.

Bahloul, D., Pereira, M., Goursat, P., Yive, N.C.K., Corriu, R.J., 1993. Preparation of silicon carbonitrides from an organosilicon polymer: I, thermal decomposition of the cross-linked polysilazane. J. Am. Ceram. Soc. 76, 1156–1162. https://doi.org/10.1111/j.1151-2916.1993.tb03734.x.

Barroso, G., Döring, M., Horcher, A., Kienzle, A., Motz, G., 2020. Polysilazane-based coatings with anti-adherent properties for easy release of plastics and composites from metal molds. Adv. Mater. Interfac. 7, 1901952 https://doi.org/10.1002/admi.201901952.

Bauer, F., Decker, U., Dierdorf, A., Ernst, H., Heller, R., Liebe, H., Mehnert, R., 2005. Preparation of moisture curable polysilazane coatings: Part I. Elucidation of low temperature curing kinetics by FT-IR spectroscopy. Prog. Org. Coating 53, 183–190. https://doi.org/10.1016/j.porgcoat.2005.02.006.

Castro, Y., Özmen, E., Durán, A., 2020. Integrated self-healing coating system for outstanding corrosion protection of AA2024. Surf. Coating. Technol. 387, 125521 https://doi.org/10.1016/j.surfcoat.2020.125521.

Chavez, R., Ionescu, E., Balan, C., Fasel, C., Riedel, R., 2011. Effect of ambient atmosphere on crosslinking of polysilazanes. J. Appl. Polym. Sci. 119, 794–802. https://doi.org/10.1002/app.32777.

Coan, T., Barroso, G., Machado, R., De Souza, F., Spinelli, A., Motz, G., 2015. A novel organic-inorganic PMMA/polysilazane hybrid polymer for corrosion protection. Prog. Org. Coating 89, 220–230. https://doi.org/10.1016/j.porgcoat.2015.09.011.

Corriu, R.J.P., Perz, R., Reye, C., 1983. Activation of silicon-hydrogen, silicon-oxygen, silicon-nitrogen bonds in heterogeneous phase. Tetrahedron 39, 999–1009. https://doi.org/10.1016/S0040-4020(01)88599-9.

D'Elia, R., Dusserre, G., Del Confetto, S., Eberling-Fux, N., Descamps, C., Cutard, T., 2018. Effect of dicumyl peroxide concentration on the polymerization kinetics of a polysilazane system. Polym. Eng. Sci. 58, 859–869. https://doi.org/10.1002/pen.24638.

D'Orazio, G., Falanga, G.E., Chazen, Z., Jones, J., Sobhani, S., 2023. Non-Oxide ceramic additive manufacturing processes for aerospace applications. In: AIAA SCITECH 2023 Forum, p. 315. https://doi.org/10.2514/6.2023-0315.

Dargère, N., Bounor-Legaré, V., Boisson, F., Cassagnau, P., Martin, G., Sonntag, P., Garois, N., 2012. Hydridosilazanes hydrolysis-condensation reactions studied by 1H and 29Si liquid NMR spectroscopy. J. Sol. Gel Sci. Technol. 62, 389–396. https://doi.org/10.1002/pen.24638.

Dursun, T., Soutis, C., 2014. Recent developments in advanced aircraft aluminium alloys. Mater. Des. 56, 862–871. https://doi.org/10.1016/j.matdes.2013.12.002, 1980-2015.

Egorkin, V.S., Vyaliy, I.E., Sinebryukhov, S.L., Gnedenkov, S.V., 2016. Duty cycle of the polarizing signal influence on morphology and properties of the PEO-coating on aluminium alloy. In: Solid State Phenomena. Trans Tech Publ, pp. 121–129. https://doi.org/10.4028/www.scientific.net/SSP.245.121.

Ely, M., Światowska, J., Seyeux, A., Zanna, S., Marcus, P., 2017. Role of post-treatment in improved corrosion behavior of trivalent chromium protection (TCP) coating

deposited on aluminum alloy 2024-T3. J. Electrochem. Soc. 164, C276. https://iopscience.iop.org/article/10.1149/2.0431706jes.
Feng, Z., Liu, Y., Thompson, G., Skeldon, P., 2010. Sol–gel coatings for corrosion protection of 1050 aluminium alloy. Electrochim. Acta 55, 3518–3527. https://doi.org/10.1016/j.electacta.2010.01.074.
Flores, O., Schmalz, T., Krenkel, W., Heymann, L., Motz, G., 2013. Selective cross-linking of oligosilazanes to tailored meltable polysilazanes for the processing of ceramic SiCN fibres. J. Mater. Chem. A 1, 15406–15415. https://doi.org/10.1039/C3TA13254D.
Furtat, P., Lenz-Leite, M., Ionescu, E., Machado, R., Motz, G., 2017. Synthesis of fluorine-modified polysilazanes via Si–H bond activation and their application as protective hydrophobic coatings. J. Mater. Chem. A 5, 25509–25521. https://doi.org/10.1039/C7TA07687H.
Gardelle, B., Duquesne, S., Vu, C., Bourbigot, S., 2011. Thermal degradation and fire performance of polysilazane-based coatings. Thermochim. Acta 519, 28–37. https://doi.org/10.1016/j.tca.2011.02.025.
Günthner, M., Wang, K., Bordia, R.K., Motz, G., 2012. Conversion behaviour and resulting mechanical properties of polysilazane-based coatings. J. Eur. Ceram. Soc. 32, 1883–1892. https://doi.org/10.1016/j.jeurceramsoc.2011.09.005.
Hafidh, A., Touati, F., Sediri, F., 2020. Synthesis, charaterization and optical properties of nanostructured silica hybrid materials obtained by soft chemistry from perhydropolysilazane/1, 2, 4-triazole precursors. J. Mol. Struct. 1218, 128496 https://doi.org/10.1016/j.molstruc.2020.128496.
Hintze, P.E., Calle, L.M., 2006. Electrochemical properties and corrosion protection of organosilane self-assembled monolayers on aluminum 2024-T3. Electrochim. Acta 51, 1761–1766. https://doi.org/10.1016/j.electacta.2005.02.147.
Hu, L., Li, M., Xu, C., Luo, Y., Zhou, Y., 2009. A polysilazane coating protecting polyimide from atomic oxygen and vacuum ultraviolet radiation erosion. Surf. Coating. Technol. 203, 3338–3343. https://doi.org/10.1016/j.surfcoat.2009.04.019.
Kong, J., Kong, M., Zhang, X., Chen, L., An, L., 2013. Magnetoceramics from the bulk pyrolysis of polysilazane cross-linked by polyferrocenylcarbosilanes with hyperbranched topology. ACS Appl. Mater. Interfaces 5, 10367–10375. https://doi.org/10.1021/am403464e.
López, A.J., Rams, J., 2015. Reinforced Sol–Gel Silica Coatings. The Sol-Gel Handbook, pp. 1207–1238. https://doi.org/10.1002/9783527670819.ch39.
Lo, T.N., Hwang, H.S., Lee, J., Park, I., 2020. Synthesis of new semi-fluorinated polysilazanes and their amphiphobic coating applications. Prog. Org. Coating 148, 105853. https://doi.org/10.1016/j.porgcoat.2020.105853.
Lo, T.N., Hong, S.W., Hwang, H.S., Park, I., 2022. Facile synthesis of fluorinated polysilazanes and their durable icephobicity on rough Al surfaces. Polymers 14, 330. https://doi.org/10.3390/polym14020330.
Macário, P.F., Vieira, A., Manfroi, L., da Silva, M.G., Leite, P., Vieira, L., 2019. Corrosion behavior of Al2024-T3, Al5052-H32, and Al6061-T6 aluminum alloys coated with DLC films in aviation fuel medium, Jet A-1 and AVGAS 100LL. Mater. Corros. 70, 2278–2291. https://doi.org/10.1002/maco.201911035.
Marceaux, S., Bressy, C., Perrin, F.-X., Martin, C., Margaillan, A., 2014. Development of polyorganosilazane–silicone marine coatings. Prog. Org. Coating 77, 1919–1928. https://doi.org/10.1016/j.porgcoat.2014.06.020.
Minevski, Z., Eylem, C., Maxey, J., Nelson, C., 2002. Polymetalate and Heteropolymetalate Conversion Coatings for Metal Substrates. Google Patents. https://patents.google.com/patent/US6500276B1/en.
Müller, S., de Hazan, Y., Penner, D., 2016. Effect of temperature, humidity and aminoalkoxysilane additive on the low temperature curing of polyorganosilazane coatings studied by IR spectroscopy, gravimetric and evolved gas analysis. Prog. Org. Coating 97, 133–145. https://doi.org/10.1016/j.porgcoat.2016.03.021.
Mussa, M.H., Rahaq, Y., Takita, S., Zahoor, F.D., Farmilo, N., Lewis, O., 2021. The influence of adding a functionalized fluoroalkyl silanes (PFDTES) into a novel silica-based hybrid coating on corrosion protection performance on an aluminium 2024-t3 alloy. Materials Proceedings 7, 6. https://doi.org/10.3390/IOCPS2021-11240.
Nguyen, T.D.H., Perrin, F.-X., Nguyen, D.L., 2013. New hybrid materials based on poly (ethyleneoxide)-grafted polysilazane by hydrosilylation and their anti-fouling activities. Beilstein J. Nanotechnol. 4, 671–677. https://doi.org/10.3762/bjnano.4.75.
Nguyen, A.S., Causse, N., Musiani, M., Orazem, M.E., Pébère, N., Tribollet, B., Vivier, V., 2017. Determination of water uptake in organic coatings deposited on 2024 aluminium alloy: comparison between impedance measurements and gravimetry. Prog. Org. Coating 112, 93–100. https://doi.org/10.1016/j.porgcoat.2017.07.004.
Ochi, M., Takahashi, R., Terauchi, A., 2001. Phase structure and mechanical and adhesion properties of epoxy/silica hybrids. Polymer 42, 5151–5158. https://doi.org/10.1016/S0032-3861(00)00935-6.
Perrin, F.-X., Nguyen, T.D.H., Nguyen, D.L., 2015. Formation, structure and antibacterial activities of silazane networks grafted with poly (ethylene glycol) branches. Prog. Org. Coating 88, 92–105. https://doi.org/10.1016/j.porgcoat.2015.06.022.
Picard, L., Phalip, P., Fleury, E., Ganachaud, F., 2015. Chemical adhesion of silicone elastomers on primed metal surfaces: a comprehensive survey of open and patent literatures. Prog. Org. Coating 80, 120–141. https://doi.org/10.1016/j.porgcoat.2014.11.022.
Salstela, J., Suvanto, M., Pakkanen, T.T., 2016. Influence of hierarchical micro-micro patterning and chemical modifications on adhesion between aluminum and epoxy. Int. J. Adhesion Adhes. 66, 128–137. https://doi.org/10.1016/j.ijadhadh.2015.12.036.
Segal, D., 1984. Sol-gel processing: routes to oxide ceramics using colloidal dispersions of hydrous oxides and alkoxide intermediates. J. Non-Cryst. Solids 63, 183–191. https://doi.org/10.1016/0022-3093(84)90397-1.
Sobhani, S., Bakhshandeh, E., Jafari, R., Momen, G., 2023. Mechanical properties, icephobicity, and durability assessment of HT-PDMS nanocomposites: effectiveness of sol–gel silica precipitation content. J. Sol. Gel Sci. Technol. 1–12. https://doi.org/10.1007/s10971-022-06033-2.
Sønderbæk-Jørgensen, R., Meier, S., Dam-Johansen, K., Skov, A.L., Daugaard, A.E., 2022. Reactivity of Polysilazanes Allows Catalyst Free Curing of Silicones. Macromolecular Materials and Engineering, 2200157. https://doi.org/10.1002/mame.202200157.
Sowntharya, L., Gundakaram, R.C., Raju, K.S., Subasri, R., 2013. Effect of addition of surface modified nanosilica into silica–zirconia hybrid sol–gel matrix. Ceram. Int. 39, 4245–4252. https://doi.org/10.1016/j.ceramint.2012.10.276.
Subasri, R., Soma Raju, K., Reddy, D., Jyothirmayi, A., Ijeri, V.S., Prakash, O., Gaydos, S. P., 2019. Environmentally friendly Zn–Al layered double hydroxide (LDH)-based sol–gel corrosion protection coatings on AA 2024-T3. J. Coating Technol. Res. 16, 1447–1463. https://doi.org/10.1007/s11998-019-00229-y.
Templin, M., Wiesner, U., Spiesss, H.W., 1997. Multinuclear solid-state-NMR studies of hybrid organic-inorganic materials. Adv. Mater. 9, 814–817. https://doi.org/10.1002/adma.19970091011.
Wang, J., Kober, D., Shao, G., Epping, J.D., Görke, O., Li, S., Gurlo, A., Bekheet, M.F., 2022. Stable anodes for lithium-ion batteries based on tin-containing silicon oxycarbonitride ceramic nanocomposites. Mater. Today Energy 26, 100989. https://doi.org/10.1016/j.mtener.2022.100989.
Xiong, L., Liu, J., Li, Y., Li, S., Yu, M., 2019. Enhancing corrosion protection properties of sol-gel coating by pH-responsive amino-silane functionalized graphene oxide-mesoporous silica nanosheets. Prog. Org. Coating 135, 228–239. https://doi.org/10.1016/j.porgcoat.2019.06.007.
Yokota, H., Imanari, N., Sugahara, Y., 2010. Formation of Si-O-N networks from silsesquiazanes. Appl. Organomet. Chem. 24, 608–611. https://doi.org/10.1002/aoc.1643.
Yuan, Q., Chai, Z.-F., Huang, Z.-R., Huang, Q., 2019. A new precursor of liquid and curable polysiloxane for highly cost-efficient SiOC-based composites. Ceram. Int. 45, 7044–7048. https://doi.org/10.1016/j.ceramint.2018.12.206.
Zhan, Y., Grottenmüller, R., Li, W., Javaid, F., Riedel, R., 2021. Evaluation of mechanical properties and hydrophobicity of room-temperature, moisture-curable polysilazane coatings. J. Appl. Polym. Sci. 138, 50469 https://doi.org/10.1002/app.50469.
Zhang, Y., Yan, C., Wang, F., Li, W., 2005. Electrochemical behavior of anodized Mg alloy AZ91D in chloride containing aqueous solution. Corrosion Sci. 47, 2816–2831. https://doi.org/10.1016/j.corsci.2005.01.010.
Zhang, X., Chen, Y., Hu, J., 2018. Recent advances in the development of aerospace materials. Prog. Aero. Sci. 97, 22–34. https://doi.org/10.1016/j.paerosci.2018.01.001.
Zhang, P., Zhang, G., Pan, J., Ma, C., Zhang, G., 2023. Non-isocyanate polyurethane coating with high hardness, superior flexibility, and strong substrate adhesion. ACS Appl. Mater. Interfaces 15, 5998–6004. https://doi.org/10.1021/acsami.2c22433.